Acta Crystallographica Section C
Crystal Structure Communications
ISSN 0108-2701

Chromium-based clinopyroxene-type germanates $NaCrGe_2O_6$ and $LiCrGe_2O_6$ at 298 K

Günther J. Redhammer,[a]* Georg Roth[b] and Georg Amthauer[a]

[a]Department of Materials Engineering and Physics, Division of Mineralogy, University of Salzburg, Hellbrunnerstrasse 34, A-5020 Salzburg, Austria, and [b]Institute of Crystallography, RWTH Aachen University, Jägerstrasse 17/19, D-52056 Aachen, Germany
Correspondence e-mail: guenther.redhammer@sbg.ac.at

Received 20 September 2008
Accepted 12 November 2008
Online 27 November 2008

The structure analyses of sodium chromium digermanate, $NaCrGe_2O_6$, (I), and lithium chromium digermanate, $LiCrGe_2O_6$, (II), provide important structural information for the clinopyroxene family, and form part of our ongoing studies on the phase transitions and magnetic properties of clinopyroxenes. (I) shows $C2/c$ symmetry at 298 K, contains one Na, one Cr (both site symmetry 2 on special position 4*e*), one Ge and three O-atom positions (on general positions 8*f*) and displays the well known clinopyroxene topology. The basic units of the structure of (I) are infinite zigzag chains of edge-sharing $Cr^{3+}O_6$ octahedra (*M*1 site), infinite chains of corner-sharing GeO_4 tetrahedra, connected to the *M*1 chains by common corners, and Na sites occupying interstitial space. (II) was found to have $P2_1/c$ symmetry at 298 K. The structure contains one Na, one Cr, two distinct Ge and six O-atom positions, all on general positions 4*e*. The general topology of the structure of (II) is similar to that of (I); however, the loss of the twofold symmetry makes it possible for two distinct tetrahedral chains, having different conformation states, to exist. While sodium is (6+2)-fold coordinated, lithium displays a pure sixfold coordination. Structural details are given and chemical comparison is made between silicate and germanate chromium-based clinopyroxenes.

Comment

The crystal chemistry of the silicate clinopyroxene minerals and their synthetic analogues has been studied in great detail (*e.g.* Cameron & Papike, 1981; Thompson *et al.*, 2005; Redhammer & Roth, 2002, 2004*a*,*b*; Redhammer *et al.*, 2005, 2006). It is now well established that the Li-bearing 1:3 clinopyroxenes (where '1' stands for the monovalent alkali cations Na^+ or Li^+, and '3' for trivalent cations such as Al^{3+}, Ga^{3+}, Cr^{3+}, Fe^{3+}, V^{3+}, Ti^{3+}, Sc^{3+}or In^{3+}) show crystallographic phase transitions as a function of temperature and pressure. Upon cooling, the high-temperature $C2/c$ modification (the most frequently found symmetry for clinopyroxenes) transforms to the low-temperature $P2_1/c$ form as described in detail for $LiFeSi_2O_6$ (Redhammer *et al.*, 2001) and for $LiMSi_2O_6$ (M = Cr^{3+}, Ga^{3+}, Sc^{3+} and V^{3+}) (Redhammer & Roth, 2004*b*). The analogous Na compounds, however, retain $C2/c$ symmetry down to low temperatures (Redhammer & Roth, 2002; Nestola *et al.*, 2007).

The clinopyroxenes have received much attention in geoscientific research, and they are beginning to attract increasing attention in solid-state physics because of their interesting magnetic properties. The titanium-based $(Na,Li)Ti^{3+}Si_2O_6$ compounds show spin-gap behaviour at low temperatures (Isobe *et al.*, 2002), and the dimerization of the chains of TiO_6 octahedra is accompanied by a crystallographic phase transition from $C2/c$ directly to $P\overline{1}$ (Redhammer *et al.*, 2003). Recently, multiferroic behaviour has been reported for clinopyroxenes $NaFeSi_2O_6$, $LiFeSi_2O_6$ and $LiCrSi_2O_6$ (Jodlauk *et al.*, 2007), and this discovery will undoubtedly further increase the interest in this important group of rock-forming minerals/materials.

Chromium-based pyroxenes are of special interest with respect to their magnetic behaviour; the competitive magnetic interaction within and between the chains of $Cr^{3+}O_6$ octahedra changes from dominating antiferromagnetic in $LiCrSi_2O_6$ and $NaCrSi_2O_6$ to pure ferromagnetic in $NaCrGe_2O_6$ (Vasiliev *et al.*, 2003, 2005; Streltsov & Khomskii, 2008). The reason for this must be attributed to the different structural topologies. $NaCrSi_2O_6$ shows the typical $C2/c$ structure (Origlieri *et al.*, 2003), while $LiCrSi_2O_6$ has $P2_1/c$ symmetry at room temperature and below, but transforms to the high-temperature HT-$C2/c$ structure at 330 K (Redhammer & Roth, 2004*b*). Except for basic structural data such as lattice parameters and symmetry (Vasiliev *et al.*, 2003, 2005) and the data given in the powder diffraction file, no further structural information is available for the chromium-based germanate clinopyroxenes. As knowledge of the structural topology of a compound is the basis for understanding its physical properties, we undertook the determination of the crystal structures of the chromium-based clinopyroxene-type compounds $NaCrGe_2O_6$, (I), and

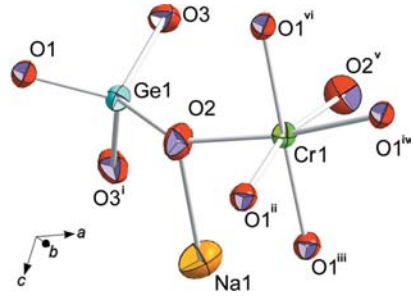

Figure 1
The asymmetric unit and symmetry-related atoms of (I), shown with 95% probability displacement ellipsoids [symmetry codes: (i) $x, -y, \frac{1}{2}+z$; (ii) $\frac{1}{2}-x, \frac{1}{2}+y, \frac{1}{2}-z$; (iii) $\frac{1}{2}+x, \frac{1}{2}-y, \frac{1}{2}+z$; (iv) $\frac{1}{2}+x, \frac{1}{2}+y, z$; (v) $1-x, y, \frac{1}{2}-z$; (vi) $\frac{1}{2}-x, \frac{1}{2}-y, -z$].

 doi:10.1107/S0108270108037633

$LiCrGe_2O_6$, (II). Comparison with $NaCrSi_2O_6$ and $LiCrSi_2O_6$ is also presented, with the structural parameters of the latter recalculated from atomic coordinates and lattice parameters given by Origlieri *et al.* (2003) and Redhammer & Roth (2004*b*).

(I) shows *C*2/*c* symmetry at 298 K and the asymmetric unit contains one distinct Na, one Cr, one Ge and three O-atom positions (Fig. 1). The compound adopts the general topology of the clinopyroxenes: infinite chains of corner-sharing GeO_4 tetrahedra (*T* sites) running parallel to the crystallographic *c* axis and related to each other by the twofold axis, zigzag chains of edge-sharing $Cr^{3+}O_6$ octahedra (*M*1 sites), also running parallel to the *c* axis, and eightfold-coordinated *M*2 sites, hosting Na^+ in the interstitial space. Compared with $NaCrSi_2O_6$ (known as the mineral kosmochlor), the replacement of Si^{4+} by Ge^{4+} causes a distinct increase in lattice parameters in the *a* and *c* directions by 3.46 and 5.08%, respectively; *b* increases by only 1.52%, while the monoclinic angle β remains almost constant. Individual bond lengths and angles are in the range typically found for the clinopyroxenes; average bond lengths, polyhedral volumes and distortion parameters are compiled in Table 1.

In (I), the *T*—O distances range between 1.717 (2) and 1.763 (2) Å, with the average of the two bridging (br) Ge1—O3 bonds $\langle T{-}O_{br}\rangle$ is 1.753 (15) Å, while the average of the two remaining nonbridging (nbr) Ge1—O bonds $\langle T{-}O_{nbr}\rangle$ is 1.735 (26) Å and the difference Δ_{br-nbr} is 0.018 Å. In $NaCrSi_2O_6$, the difference Δ_{br-nbr} is 0.025 Å. According to Ohashi (1981) and Ohashi *et al.* (1990), the difference Δ_{br-nbr} is related to the electronegativity of the M^{3+} cation within the series Sc–Ti–V–Cr–Al; Δ_{br-nbr} decreases with increasing electronegativity of the M^{3+} cation. From this finding, it could be concluded that Cr^{3+} acts as a more electronegative centre in (I) than in $NaCrSi_2O_6$. The GeO_4 tetrahedra are elongated along *a**. This is shown by the angle τ, which is defined as the mean of the three $O_{basal}{-}T{-}O_{apex}$ bond angles. Ideal tetrahedra have $\tau = 109.47^\circ$, while this value is 112.65 (11)° in (I) (Table 1). By nature, the most distinct differences between the germanate (I) and silicate $NaCrSi_2O_6$ clinopyroxene concern the tetrahedral sites. The $\langle T{-}O\rangle$ distance in the germanate is larger by 0.118 Å compared with the silicate; this corresponds well with the difference in ionic radius between Si^{4+} and Ge^{4+} (0.14 Å; Shannon & Prewitt, 1969). A similar difference of 0.122 Å in $\langle T{-}O\rangle$ distances was observed for analogous *C*2/*c* $CaZnGe_2O_6$ and $CaZnSi_2O_6$ clinopyroxenes (Redhammer & Roth, 2005). The GeO_4 tetrahedra are more elongated along *a** compared with the SiO_4 tetrahedron (Table 1) and thus show a distinctly larger tetrahedral quadratic elongation (TQE) and a larger tetrahedral angle variance (TAV, Table 1). From this, it is apparent that $NaCrSi_2O_6$ possesses a more regular tetrahedral environment than does (I). While bond lengths and angles generally show little variation with changes in composition, temperature or pressure, the O3—O3—O3 bridging angle, defining the conformation state of the chains, changes significantly with changes in parameters of state. In (I), the tetrahedral chains show an '*O*' rotation (O3—O3—O3 < 180°; Redhammer & Roth, 2004*b*) and the tetrahedral bridging angle is 170.57 (9)°. Compared with $NaCrSi_2O_6$ (O3—O3—O3 = 172.81°), the tetrahedral chains are more kinked in the germanate as this favours the matching of the larger GeO_4 tetrahedra to the $Cr^{3+}O_6$ octahedral chain. The increased kink of the tetrahedral chains is also responsible for the smaller increase in the *b* lattice parameter upon substitution of Si^{4+} by Ge^{4+}. As the *T*—O bonds do not expand as much as might be expected from the different ionic radii of Si^{4+} and Ge^{4+}, this can be regarded (besides tetrahedral chain kinking) as an additional mechanism for maintaining the size comparability between tetrahedral and octahedral chains.

The *M*2 site shows a (6+2)-fold coordination in (I), with six bonds ranging between 2.404 (3) and 2.486 (2) Å; the remaining two $Na1{-}O3^{vii}$ and $Na1{-}O3^{v}$ bonds are 2.764 (3) Å, contributing 0.07 valence units (v.u.) to the bond valence sum (S) of Na^+ [symmetry codes: (v) $-x+1, y, -z+\frac{1}{2}$; (vii) $x, y, z+1$]. The total bond valence sum (Brese & O'Keeffe, 1991) at the *M*2 site is S = 1.21 v.u., indicating that the *M*2 site in (I) is distinctly overbonded. Both the volume of this irregularly shaped *M*2 polyhedron and the $\langle Na{-}O\rangle$ bond lengths are somewhat larger in (I) compared with $NaCrSi_2O_6$, showing that the available space for the *M*2 site is larger in (I).

Most interesting in terms of the magnetic properties is the topology of the *M*1 site. By sharing common edges, the $Cr^{3+}O_6$ octahedra form a quasi-one-dimensional zigzag chain along *c* (Fig. 2), with an average $\langle Cr^{3+}{-}O\rangle$ distance of 2.004 (2) Å in (I) (Table 1). Both average and individual Cr1—O bonds are larger by 0.01 Å (~0.5%) in (I) and the CrO_6 octahedra are somewhat more elongated along the *c* axis compared with isostructural $NaCrSi_2O_6$. This can be deduced from the larger $O1^{vi}{-}Cr1{-}O1^{iii}$ bond angle of 176.8 (13)° in (I) compared with 173.1 (1)° in $NaCrSi_2O_6$ [symmetry codes: (iii) $x+\frac{1}{2}, -y+\frac{1}{2}, z+\frac{1}{2}$; (vi) $-x+\frac{1}{2}, -y+\frac{1}{2}, -z$]. While the bond-length distortion (BLD) is similar in (I) and $NaCrSi_2O_6$, the germa-

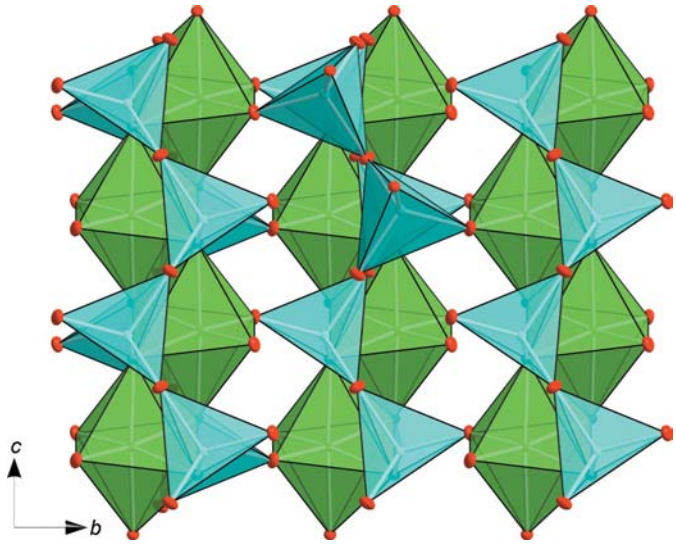

Figure 2
Polyhedral representation of the *C*2/*c* structure of (I), displaying the *M*1 octahedral chains and related GeO_4 tetrahedra. Na sites have been omitted for clarity.

nate compound shows distinctly larger values for the angular variance and the quadratic elongation (OAV and OQE in Table 1). This is mainly due to distinct alterations in octahedral O—O atom edges. Here, the most pronounced changes can be found for the $O1^{vi}$—$O1^{ii}$ and $O2$—$O2^{v}$ edges [symmetry code: (ii) $-x+\frac{1}{2}, y+\frac{1}{2}, -z+\frac{1}{2}$], which increase by as much as 3.8 and 4.9%, respectively, from $NaCrSi_2O_6$ to (I). As Cr1—O bond lengths do not alter much, consequently the O—Cr1—O bond angles involving the $O1^{vi}$—$O1^{ii}$ and $O2$—$O2^{v}$ edges also show marked increases by 4.3 and 5.9% upon the replacement of Si^{4+} by Ge^{4+}. The aforementioned O atoms are common to both the CrO_6 octahedra and four neighbouring tetrahedral sites, and thus are sensitive to changes in the tetrahedral cation size. As a third mechanism for maintaining the match between octahedral and tetrahedral chains, octahedral edge-length and bond-angle variation is active at the *M*1 site, rather than Cr^{3+}—O bond-length stretching.

The increased elongation of the CrO_6 octahedra in (I) causes a size reduction of the common $O1^{ii}$—$O1^{ix}$ edge between two neighbouring CrO_6 octahedra from 2.606 (2) to 2.578 (2) Å in $NaCrSi_2O_6$ and (I), respectively; the $O1^{iii}$—Cr1—$O1^{ii}$ angle opposite this O1—O1 edge decreases from 80.4 (1) to 78.76 (10)°. A direct consequence of this is a larger separation of Cr^{3+}—Cr^{3+}pairs within the chain and a change in the Cr1—$O1^{ii,iii}$—$Cr1^{viii}$ angle, which is important for the magnetic super-exchange interaction *via* the common O1 oxygen: the Cr—Cr^{viii} interatomic distance within the *M*1 chain increases from 3.086 (1) Å in $NaCrSi_2O_6$ to 3.140 (1) Å in (I), and the Cr1—$O1^{ii,iii}$—$Cr1^{viii}$ angle from 99.6 (1) to 101.2 (1)° [symmetry code: (viii) $-x+1, -y+1, -z+1$]. Also, the separation between neighbouring *M*1 chains is distinctly larger in (I): the shortest contact between two Cr^{3+} ions in two different *M*1 chains is 5.549 (1) Å in $NaCrSi_2O_6$, but increases to 5.666 (1) Å in the germanate. These differences in bonding topologies certainly influence magnetic properties in chromium-based clinopyroxenes at low temperatures.

(II) adopts $P2_1/c$ symmetry at room temperature with one distinct Li, one Cr, two Ge and six O-atom positions in the asymmetric unit (Fig. 3). The general topology of the $P2_1/c$ structure in (II) is similar to the *C*2/*c* structure of (I); the main difference is the presence of two distinct tetrahedral chains, *A* and *B*, due to the loss of the twofold axis, with slightly different bond lengths and angles and distinctly different kinking states of the two independent GeO_4 chains (Fig. 4). The *A* chain is '*S*'-rotated, having a tetrahedral bridging angle of 209.7 (1)°, while the *B* chain is '*O*'-rotated with a bridging angle of 136.6 (1)°. It is evident that the tetrahedral chains in (II) exhibit a distinct kinking, which is far larger than in (I) or in the $P2_1/c$ phase of $LiCrSi_2O_6$ (Table 1). Similar small bridging angles were found in $ZnSiO_3$ [139.7 (9)° for the *B* chain; Arlt & Angel, 2000] and clinoenstatite $Ca_{0.15}Mg_{1.85}Si_2O_6$ [143.0 (1)° for the *B* chain; Tribaudino *et al.*, 2002], but not in 1:3 clinopyroxenes.

In (II), the tetrahedra of the *B* chain have similar $\langle T-O\rangle$ and $\langle O-O\rangle_T$ bond lengths with similar BLD_T values and a similar polyhedral volume (Table 1), while the distortion parameters are smaller compared with the tetrahedra of the *A* chain; thus, despite the distinct kinked state, the tetrahedra of the *B* chain appear to be more regular. Both *T* sites in (II) are elongated along *a**; the elongation is smaller for the *B*-chain tetrahedra and is very similar to that found for the SiO_4 tetrahedra in the *B* chain of $LiCrSi_2O_6$. The polyhedral distortions are also very similar in both compounds for the *B*-chain tetrahedra, though there is the size difference due to different tetrahedral cations. The *A*-chain tetrahedra are distinctly elongated [τ = 111.64 (10)°] and reveal the largest deviations from ideal geometry of the chromium-based 1:3 clinopyroxenes; in particular, the bond-angle variance is high (Table 1). As in all clinopyroxenes, the bridging *T*—O bond lengths are longer than the two nonbridging bonds; the difference Δ_{br-nbr} is 0.016 (2) Å for the *A* chain and 0.021 (2) Å for the *B* chain. Bond valence sums (Brese & O'Keeffe, 1991) for the tetrahedral site in (II) are close to the

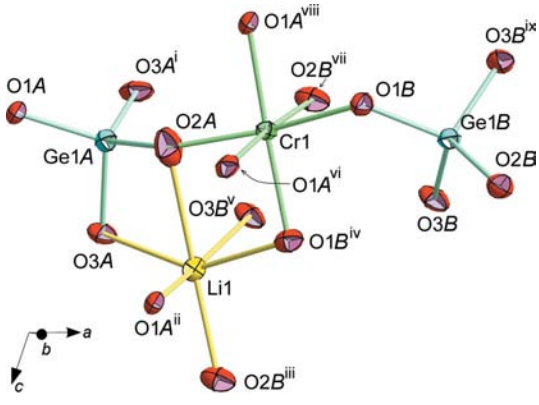

Figure 3
The asymmetric unit and symmetry-related atoms of (II), showing 95% probability displacement ellipsoids [symmetry codes: (i) $x, \frac{1}{2}-y, -\frac{1}{2}+z$; (ii) $-x, 1-y, 1-z$; (iii) $1-x, -\frac{1}{2}+y, \frac{3}{2}-z$; (iv) $x, \frac{3}{2}-y, \frac{1}{2}+z$; (v) $1-x, 1-y, 1-z$; (vi) $-x, \frac{1}{2}+y, \frac{1}{2}-z$; (vii) $1-x, -\frac{1}{2}+y, \frac{1}{2}-z$; (viii) $-x, 1-y, -z$; (ix) $x, \frac{3}{2}-y, -\frac{1}{2}+z$].

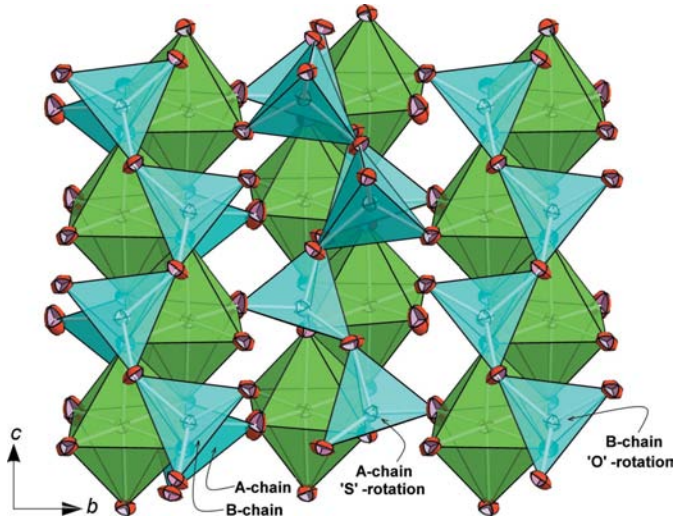

Figure 4
Polyhedral representation of the $P2_1/c$ structure of (II), showing the *M*1 octahedral chains and related GeO_4 tetrahedra. Li sites have been omitted for clarity. A similar orientation to that in Fig. 2 was chosen to facilitate comparison.

ideal value; the *A*-site Ge is slightly overbonded and the *B*-site Ge slightly underbonded. The bridging O3*A* atom shows a valence sum of S = 2.14 v.u.; in the *B*-chain, S is almost ideal for O3*B* (2.02 v.u.).

While the *M*2 site in (I) has a (6+2)-fold coordination, in (II) the coordination is purely sixfold. The Li1—O bonds range between 2.038 (6) and 2.369 (6) Å; the next nearest O atoms are 3.144 (6) and 3.478 (6) Å from Li^+ and cannot be regarded as bonding atoms. The sixfold O-atom environment of Li^+ in (II), however, is far from being ideal octahedral, and gives rise to extreme values for the distortion parameters OAV (198.5°) and OQE (1.0576). The coordination of Li^+ in (II) is different from that in $LiCrSi_2O_6$ in the $P2_1/c$ form: in the latter, five bonds lie between 2.078 (6) and 2.313 (6) Å, but two O3*B* atoms are found at somewhat larger distances of 2.678 (6) and 2.891 (6) Å, giving rise to a (5+2)-fold coordination in $LiCrSi_2O_6$. This non-uniform Li1—O bond distribution is related to the conformation state of the tetrahedral chain. The distinct kinking of the *B* chain in (II) brings one O3*B* atom closer to the Li^+ atom, but moves the other one out of the coordination sphere. In addition, the Li1—O2 distances are evidently different in the silicate and the germanate, reflecting the different topologies of the CrO_6 site.

The individual Cr1—O, ⟨Cr1—O⟩ and $\langle O-O\rangle_{M1}$ distances in (II) are similar to the values found in $NaCrSi_2O_6$ and $LiCrSi_2O_6$, and are only slightly smaller than those in (I) (Table 1). The CrO_6 octahedra in (II) are again elongated along *c* ($\langle Cr1-O\rangle_{apex}/\langle Cr1-O\rangle_{equatorial} > 1$; Table 1); the angle $O1A^{viii}—Cr1—O1B^{iv}$ is 176.1 (1)° and thus almost identical to $LiCrSi_2O_6$ and (I) and close to the ideal value of 180° for the undistorted octahedron [symmetry codes: (iv) x, $-y+\frac{3}{2}$, $z+\frac{1}{2}$; (viii) $-x$, $-y+1$, $-z$]. The bond-length distortion is larger in (II) compared with the sodium pyroxene, while the angular distortion is smaller; however, the latter is still distinctly larger than in the silicates (Table 1). The replacement of Si^{4+} by Ge^{4+} influences the O—O edges of the CrO_6 octahedron in a different way. An increase in the O···O interatomic distances across octahedral edges is observed *e.g.* for the $O1A^{viii}—O1A^{vi}$, the $O2A—O2B^{vii}$ or the $O1B—O1B^{iv}$ edges. These increases are in the range 1.0–1.5% (0.03–0.05 Å) and are responses to the increase in the ionic size of the tetrahedral cation; however, there are O—O edges that show a distinct decrease in lengths, among them the $O1A^{vi}—O2A$ edge which is shortened by 3.0% and the $O1A^{viii}—O2B^{vii}$ edge, being shorter by 2.7% in the germanate compound [symmetry codes: (vi) $-x$, $y+\frac{1}{2}$, $-z+\frac{1}{2}$; (vii) $-x+1$, $y-\frac{1}{2}$, $-z+\frac{1}{2}$]. The latter alterations can be related to the different conformation of the tetrahedral chains in (II) and $LiCrSi_2O_6$, respectively, which causes, by counter-rotation, a compression of the O—O edges. In contrast, the $O2B^{vii}—O1B^{iv}$ edge is increased by 3.2% in (II) relative to $LiCrSi_2O_6$ due to the distinct kinking of the tetrahedral chains.

The common edges between neighbouring octahedra, *viz.* $O1A^{viii}—O1B$ and $O1B^{iv}—O1A^{vii}$, are also shorter in (II) compared with $LiCrSi_2O_6$ [2.624 (5) and 2.654 (7) Å, respectively], and the angles opposite these edges are smaller in the germanate. The shortest distance between $Cr^{3+}—Cr^{3+}$ pairs within the *M*1 chain is increased from 3.064 (1) Å in $LiCrSi_2O_6$ to 3.098 (1) Å in (II), and thus is also larger than in $NaCrSi_2O_6$ (Table 1). Within the $P2_1/c$ structure, two different Cr1—O1—Cr1 angles exist: the larger includes the $O1A^{vi}$ atom with $Cr—O1A^{vi}—Cr^{iv}$ = 100.2 (1)°, the smaller one includes the $O1B^{ii}$ atom with $Cr—O1B^{iv}—Cr^{iv}$ = 98.7 (1)°. In $LiCrSi_2O_6$, these two corresponding angles are 98.4 (1) and 98.1 (1)°, respectively. Magnetic super-exchange between Cr^{3+} ions within the *M*1 chains takes place *via* the aforementioned two O atoms. The interchain separation (nearest distance between two Cr^{3+} ions in different chains) is distinctly larger in (II) and takes a value close to that found in (I) (Table 1). The bond valence sums at the Cr sites are close to the ideal value of 3+ both in (II) and in $LiCrSi_2O_6$, while in (I) Cr^{3+} appears to be slightly underbonded (Table 1). The difference Δ_{br-nbr} in (II) is somewhat smaller for the Ge*A* site, indicating a more electropositive character; this could indicate that electrons of Cr^{3+} ($3d^3$ configuration) are delocalized towards the bridging O atoms between the Cr1 and the Ge1*A* sites, *e.g.* towards $O1A^{vi}$ in Fig. 3, the corresponding Ge1*A* site being $Ge1A^{vi}$. Such a localization would result in high screening constants in the direction of $O1A^{vi}$ and in an increment in the electric charge of the associated O1*A* atoms. Indeed, the valence sums are largest among the octahedral O atoms for the O1*A* atoms (S = 2.04 v.u.), while S is 1.98, 1.82 and 1.86 for the O1*B*, O2*A* and O2*B* atoms, respectively. High screening constants indicate electropositive character and increased charge on oxygen is accompanied by increasing repulsion effects.

From the data presented here, some basic structural conclusions concerning the magnetic properties of chromium-based clinopyroxenes can be derived: (I) with a proposed ferromagnetic (FM) ordering has by far the largest $Cr^{3+}—Cr^{3+}$ separation within [3.140 (1) Å] and between [5.666 (1) Å] the *M*1 chains, and the super-exchange pathway within the *M*1 chain shows the largest deviation from a 90° Cr—O—Cr angle, which would favour antiferromagnetic (AFM) interactions (Goodenough, 1955). On the other hand, the silicate $LiCrSi_2O_6$, which shows the highest magnetic ordering temperature and a distinctly negative paramagnetic Curie temperature (standing for an overall antiferromagnetic character of the ordering), has the smallest $Cr^{3+}—Cr^{3+}$ contacts and the smallest Cr—O—Cr angle. Increasing the inter- and intrachain separation of Cr^{3+} ions may thus weaken AFM and favour FM interaction. This could be the reason for the change in the overall magnetic property from dominating antiferromagnetic in $LiCrSi_2O_6$ to dominating ferromagnetic in (I). However, the exact spin structure within and between the chains remains unclear and can only be extracted by detailed neutron diffraction experiments.

Experimental

The title compounds were synthesized by the flux growth technique. Mixtures of the oxides Na_2CO_3/Li_2CO_3, Cr_2O_3 and GeO_2 (finely ground and homogenized) in the exact stoichiometry of the title compounds were added to the high-temperature solvent. Tests with

molybdate/vanadate fluxes under atmospheric conditions appeared to be unsuccessful, while experiments with a molar mixture of 1 NaF/LiF, 0.5 V_2O_5 and 0.1 PbO as flux turned out to give good yields of high-quality single crystals up to 1 mm in size. A flux-to-nutrient ratio of 2:1 gave the best results for both compounds. Each mixture was placed in a platinum crucible, covered with a lid, heated to 1373 K over a period of 12 h, kept at this temperature for 24 h and then cooled to 973 K at a rate of 2 K h^{-1}. The resulting single crystals were emerald green and showed a short prismatic habit.

Compound (I)

Crystal data

$NaCrGe_2O_6$
M_r = 316.17
Monoclinic, $C2/c$
a = 9.9151 (8) Å
b = 8.8441 (7) Å
c = 5.4595 (4) Å
β = 107.548 (1)°
V = 456.47 (6) Å^3
Z = 4
Mo $K\alpha$ radiation
μ = 15.47 mm^{-1}
T = 295 (2) K
0.14 × 0.12 × 0.08 mm

Data collection

Bruker SMART APEX diffractometer
Absorption correction: numerical *via* equivalents using *X-SHAPE* (Stoe & Cie, 1996)
T_{min} = 0.13, T_{max} = 0.285
2696 measured reflections
559 independent reflections
548 reflections with $I > 2\sigma(I)$
R_{int} = 0.043

Refinement

$R[F^2 > 2\sigma(F^2)]$ = 0.021
$wR(F^2)$ = 0.056
S = 1.19
559 reflections
48 parameters
$\Delta\rho_{max}$ = 0.73 e Å^{-3}
$\Delta\rho_{min}$ = −0.58 e Å^{-3}

Compound (II)

Crystal data

$LiCrGe_2O_6$
M_r = 300.12
Monoclinic, $P2_1/c$
a = 9.7989 (7) Å
b = 8.7190 (7) Å
c = 5.3410 (4) Å
β = 108.905 (4)°
V = 431.70 (6) Å^3
Z = 4
Mo $K\alpha$ radiation
μ = 16.25 mm^{-1}
T = 295 (2) K
0.14 × 0.13 × 0.07 mm

Data collection

Bruker SMART APEX diffractometer
Absorption correction: numerical *via* equivalents using *X-SHAPE* (Stoe & Cie, 1996)
T_{min} = 0.12, T_{max} = 0.295
5160 measured reflections
1064 independent reflections
1001 reflections with $I > 2\sigma(I)$
R_{int} = 0.051

Refinement

$R[F^2 > 2\sigma(F^2)]$ = 0.026
$wR(F^2)$ = 0.068
S = 1.12
1064 reflections
92 parameters
$\Delta\rho_{max}$ = 1.35 e Å^{-3}
$\Delta\rho_{min}$ = −0.71 e Å^{-3}

For (I), structure solution using Patterson methods (Sheldrick, 2008) yielded all metal and O-atom positions. Two additional data collections on crystals of different experimental runs gave identical structural parameters. Systematic absences indicated the space group $P2_1/c$ for (II), which is the same as that found for the analogous compound $LiCrSi_2O_6$ at room temperature. The structure solution for (II) using Patterson methods gave the Ge-, Cr- and all O-atom positions, while Li was located from difference Fourier map analysis.

For both compounds, data collection: *SMART* (Bruker, 2001); cell refinement: *SAINT-Plus* (Bruker, 2001); data reduction: *SAINT-*

Table 1
Selected structural and polyhedral distortion parameters for (I) and (II) in comparison with the corresponding silicates.

Data for $NaCrSi_2O_6$ were calculated from the atomic coordinates and lattice parameters of Origlieri *et al.* (2003). Data for $LiCrSi_2O_6$ in $P2_1/c$ were calculated from the atomic coordinates and lattice parameters of Redhammer & Roth (2004*b*) at T = 303 K. Data for $LiCrSi_2O_6$ in $C2/c$ were calculated from the atomic coordinates and lattice parameters of Redhammer & Roth (2004*b*) at T = 348 K.

	(I) $C2/c$	$NaCrSi_2O_6$ $C2/c$	(II) $P2_1/c$	$LiCrSi_2O_6$ $P2_1/c$	$LiCrSi_2O_6$ $C2/c$
T_N (K)†	6	3	3.7	11	11
Θ_P (K)†	13	−0.3	−5.7	−28.7	−28.7
⟨Cr1—O⟩ (Å)	2.004 (2)	1.993	1.995 (2)	1.992	1.991
⟨O—O⟩$_{M1}$ (Å)	2.831 (2)	2.817	2.816 (2)	2.813	2.812
Volume$_{M1}$ (Å^3)	10.48 (1)	10.42	10.39 (1)	10.42	10.39
BLD‡$_{M1}$ (%)	1.79 (5)	1.75	2.40 (5)	2.35	2.34
OAV§$_{M1}$ (°)	54.30 (9)	29.41	43.29 (9)	27.29	30.16
OQE¶$_{M1}$	1.0164	1.0090	1.0133	1.0089	1.0095
S††$_{M1}$ (v.u.)	2.83 (4)	n.d.	2.92 (3)	2.93	2.99
Cr1—Cr1$_{(intra)}$ (Å)	3.140 (1)	3.086	3.098 (1)	3.064	3.066
Cr1—Cr1$_{(inter)}$ (Å)	5.666 (1)	5.459	5.591 (1)	5.364	5.343
Cr1—O1—Cr1 (°)	101.2 (1)	99.6	100.2 (1)	98.4	98.3
Cr1—O1—Cr1 (°)			98.7 (1)	98.1	
⟨Cr1—O⟩$_{apex}$ /⟨Cr1—O⟩$_{equatorial}$	1.009 (3)	1.008	1.011 (3)	1.004	1.008
⟨*M*2—O⟩ (Å)	2.525 (3)	2.492	2.184 (7)	2.245	2.234
⟨O—O⟩$_{M2}$ (Å)	3.065 (3)	3.034	3.059 (5)	3.014	2.995
Volume$_{M2}$ (Å^3)	26.52 (2)	25.44	12.83 (4)	10.86	10.89
S††$_{M2}$ (v.u.)	1.21 (3)	n.d.	0.91 (3)	0.82	0.81
Chain *A*					
⟨*T*—O⟩ (Å)	1.744 (2)	1.626	1.743 (2)	1.619	1.620
⟨O—O⟩$_T$ (Å)	2.842 (2)	2.653	2.840 (2)	2.643	2.644
BLD‡$_T$ (%)	0.83 (5)	1.09	0.98 (5)	1.02	0.96
Volume$_T$ (Å^3)	2.70 (1)	2.20	2.68 (1)	2.17	2.17
TAV‡‡ (°)	25.09 (5)	16.57	32.58 (5)	13.02	12.62
TQE§§	1.0063	1.0040	1.0088	1.0034	1.0033
τ¶¶ (°)	112.65 (11)	110.65	111.64 (10)	110.23	110.42
O3—O3—O3 (°)	170.57 (9)	172.81	209.69 (9)	191.47	180.92
T—O—*T* (°)	133.2 (1)	140.2	127.2 (1)	140.1	141.8
S††$_T$ (v.u.)	4.05 (3)	n.d.	4.06 (3)	4.05	4.05
Δ_{br-nbr}(Å)	0.018 (2)	0.025	0.016 (2)	0.012	0.006
Chain *B*					
⟨*T*—O⟩ (Å)			1.750 (2)	1.621	
⟨O—O⟩$_T$ (Å)			2.856 (2)	2.645	
BLD$_T$ (%)			1.02 (5)	0.99	
Volume$_T$ (Å^3)			2.73 (1)	2.175	
TAV‡‡ (°)			18.39 (6)	11.68	
TQE§§			1.0045	1.0030	
τ¶¶ (°)			110.11 (9)	110.12	
O3—O3—O3 (°)			136.61 (9)	164.69	
T—O—*T* (°)			124.2 (1)	140.31	
S††$_T$ (v.u.)			3.98 (4)	4.04	
Δ_{br-nbr} (Å)			0.021 (2)	0.009	

† Data taken from Vasiliev *et al.* (2005). ‡ Bond-length distortion (BLD) = $(100/n)\sum_{i=1}^{n}[|(X-O)_i - \langle X-O\rangle|]/\langle X-O\rangle)]$, with n = number of bonds, $(X-O)_i$ = central cation to oxygen length and $\langle X-O\rangle$ = average cation–oxygen bond length (Renner & Lehmann, 1986). § Octahedral angle variance (OAV) = $\sum_{i=1}^{n}(\Theta_i - 90)^2/11$ (Robinson *et al.*, 1971). ¶ Octahedral quadratic elongation (OQE) = $\sum_{i=1}^{6}(l_i/l_o)^2/6$ with l_o = centre to vertex distance for a regular octahedron whose volume is equal to that of the undistorted octahedron with bond length l_i (Robinson *et al.*, 1971). †† Bond valence sum (S) (Brese & O'Keeffe, 1991). ‡‡ Tetrahedral angle variance (TAV) = $\sum_{i=1}^{n}(\Theta_i - 109.47)^2/5$ (Robinson *et al.*, 1971). §§ Tetrahedral quadratic elongation (TQE) = $\sum_{i=1}^{4}(l_i/l_t)^2/4$ with l_t = centre to vertex distance for a regular tetrahedron whose volume is equal to that of the undistorted tetrahedron with bond length l_i (Robinson *et al.*, 1971). ¶¶ τ = mean of the three $O_{basal}—T—O_{apex}$ angles.

Plus; program(s) used to solve structure: *SHELXS97* (Sheldrick, 2008); program(s) used to refine structure: *SHELXL97* (Sheldrick, 2008); molecular graphics: *DIAMOND* (Brandenburg, 1999); software used to prepare material for publication: *WinGX* (Farrugia, 1999).

GJR gratefully acknowledges financial support by the Fonds zur Förderung der Wissenschaftlichen Forschung (FWF), Vienna, Austria, under grant Nos. R33-N10 (Erwin Schrödinger Rückkehr Stipendium) and P19762-N10.

Supplementary data for this paper are available from the IUCr electronic archives (Reference: FA3169). Services for accessing these data are described at the back of the journal.

References

Arlt, T. & Angel, R. J. (2000). *Phys. Chem. Miner.* **27**, 719–731.
Brandenburg, K. (1999). *DIAMOND*. Crystal Impact GbR, Bonn, Germany.
Brese, N. E. & O'Keeffe, M. (1991). *Acta Cryst.* B**47**, 192–197.
Bruker (2001). *SMART* (Version 5.6) and *SAINT-Plus* (Version 5.0). Bruker AXS Inc., Madison, Wisconsin, USA.
Cameron, M. & Papike, J. J. (1981). *Am. Mineral.* **66**, 1–50.
Farrugia, L. J. (1999). *J. Appl. Cryst.* **32**, 837–838.
Goodenough, J. B. (1955). *Phys. Rev.* **100**, 564–573.
Isobe, M., Ninomiya, E., Vasiliev, A. E. & Ueda, Y. (2002). *J. Phys. Soc. Jpn*, **71**, 1423–1426.
Jodlauk, S., Becker, P., Mydosh, J. A., Khomskii, D. I., Lorenz, T., Streltsov, S. V., Hezel, D. C. & Bohaty, L. (2007). *J. Phys. Condens. Matter*, **19**, 432201.
Nestola, F., Rotiroti, N., Bruno, M., Tribaudino, M., van Smaalen, S., Ohashi, H. & Redhammer, G. J. (2007). *Am. Mineral.* **92**, 560–569.
Ohashi, H. (1981). *J. Jpn Assoc. Min. Petr. Econ. Geol.* **76**, 308–311.
Ohashi, H., Osawa, T. & Sato, A. (1990). *Acta Cryst.* B**46**, 742–747.
Origlieri, M. J., Downs, R. T., Thompson, R. M., Pommier, C. J. S., Denton, M. B. & Harlow, G. E. (2003). *Am. Mineral.* **88**, 1025–1032.
Redhammer, G. J., Amthauer, G., Roth, G., Tippelt, G. & Lottermoser, W. (2006). *Am. Mineral.* **91**, 1271–1292.
Redhammer, G. J., Ohashi, H. & Roth, G. (2003). *Acta Cryst.* B**59**, 730–746.
Redhammer, G. J. & Roth, G. (2002). *Z. Kristallogr.* **217**, 63–72.
Redhammer, G. J. & Roth, G. (2004*a*). *Z. Kristallogr.* **219**, 278–294.
Redhammer, G. J. & Roth, G. (2004*b*). *Z. Kristallogr.* **219**, 585–605.
Redhammer, G. J. & Roth, G. (2005). *Acta Cryst.* C**61**, i20–i22.
Redhammer, G. J., Roth, G., Paulus, W., Andé, G., Lottermoser, W., Amthauer, G., Treutmann, W. & Koppelhuber-Bitschnau, B. (2001). *Phys. Chem. Miner.* **78**, 337–346.
Redhammer, G. J., Tippelt, G., Merz, M., Roth, G., Treutmann, W. & Amthauer, G. (2005). *Acta Cryst.* B**61**, 367–380.
Renner, B. & Lehmann, G. (1986). *Z. Kristallogr.* **175**, 43–59.
Robinson, K., Gibbs, G. V. & Ribbe, P. H. (1971). *Science*, **172**, 567–570.
Shannon, R. D. & Prewitt, C. T. (1969). *Acta Cryst.* B**25**, 925–946.
Sheldrick, G. M. (2008). *Acta Cryst.* A**64**, 112–122.
Stoe & Cie (1996). *X-SHAPE* and *X-RED*. Stoe & Cie, Darmstadt, Germany.
Streltsov, S. V. & Khomskii, D. I. (2008). *Phys. Rev. B*, **77**, 064405.
Thompson, R. M., Downs, R. T. & Redhammer, G. J. (2005). *Am. Mineral.* **90**, 1840–1851.
Tribaudino, M., Nestola, F., Cámara, F. & Domeneghetti, M. C. (2002). *Am. Mineral.* **87**, 648–657.
Vasiliev, A. N., Ignatchik, O. L., Sokolov, A. N., Horoi, Z., Isobe, M. & Ueda, Y. (2003). *JETP Lett.* **78**, 551–554.
Vasiliev, A. N., Ignatchik, O. L., Sokolov, A. N., Horoi, Z., Isobe, M. & Ueda, Y. (2005). *Phys. Rev. B*, **72**, 012412.